# Chapter 3

# Minimum Operator Based Data Driven Control

## 3.1 Introduction

Data-driven approaches have emerged as a popular research domain and have been applied to numerous real-world applications [49]. DDC methods can be broadly categorized into two main approaches. The first approach involves using a predefined transfer function for the controller, where its structure remains fixed while the numerical parameters are directly adjusted based on insights obtained from measured data [13]. The second approach focuses on designing a generic controller using function approximations, which may include techniques such as neural networks or Taylor series approximations. In this case, the controller parameters are fine-tuned by minimizing a specified performance criterion, utilizing both offline and online input-output data [14], a concept popularized as model-free adaptive control (MFAC). In this chapter, we have used a concept called the pseudo partial derivative (PPD) and pseudo gradient (PG) an approaches to capture the dynamic behavior of the controlled plant, moving away from the traditional state-space representation. This framework includes three different dynamic linearization data models [14]: compact-form dynamic linearization (CFDL), partial-form dynamic linearization (PFDL), and full-form dynamic linearization (FFDL). These models offer equivalent representations of system dynamics, focusing on how changes in the control input and other influencing factors affect the system's output.

In [14], MFAC method utilizing CFDL data-driven modeling is presented. This ap-

proach designs controllers and analyzes closed-loop systems using only measured I&O, without relying on dynamics. Linearizing the nonlinear system using CFDL, a new non-affine system is established, which contains an unknown nonlinear term and a linear parametric term affine to the control input and preceding output data. Thus, it is necessary to address the influence of the unknown nonlinear term on the system effectively. The fusion of CFDL with a DSMC framework is effective in handling such nonlinearities. The concept of model-free adaptive sliding mode control, which combines MFAC with DSMC, was first introduced in [15], though it did not account for disturbances and system uncertainties. Building on this, [16] proposes an adaptive DSMC using CFDL for a class of discrete nonlinear systems. Recently, minimum operator approach has been extended to the discrete sliding mode domain, with notable advancements in DSMC [50], [2] as MDSMC. This chapter proposes the following novelties for nonlinear DTS with perturbations using DDC framework:

- Design of controllers by combining the CFDL approach with minimum-operator-based MDSMC.
- The proposed data-driven control laws ensure finite-time boundedness of the switching function and reduced quasi-sliding mode domain (QSMD), offering improved robust control compared to previous approaches.

## 3.2 CFDL Data Model & Disturbance Estimation

A MIMO discrete-time nonlinear system can be represented as:

$$y_{k+1} = f\left(y_k, y_{k-1}, \ldots, y_{k-n_y}, u_k, u_{k-1}, \ldots, u_{k-n_u}\right) + \delta_k \tag{3.1}$$

$y_k \in R^n$ and $u_k \in R^n$ denote the output and input of the dynamics, respectively; $n_y > 0$, $n_u > 0$ where $n_y, n_u \in \mathbb{Z}^+$ are unknown. $\delta_k$ denotes the constrained perturbations such that $\|\delta_k\| \leq \mathcal{D}$, where $\mathcal{D} > 0$. The function $f(\cdot)$ characterizes the DTS, such that:

$$z_{k+1} = f\left(y_k, y_{k-1}, \ldots, y_{k-n_y}, u_k, u_{k-1}, \ldots, u_{k-n_u}\right) \tag{3.2}$$

Accordingly, (3.1) can be expressed as

$$y_{k+1} = z_{k+1} + \delta_k \tag{3.3}$$

**Assumption 1.** The system described by (3.1) exhibits both controllability and observability. In particular, if the target signal $y'_{k+1}$ remains bounded, it follows that the control input $u_k$ will also be constrained, allowing $y_{k+1}$ to accurately track the desired signal $y'_{k+1}$.

**Assumption 2.** The partial derivative $\frac{\partial f(\cdot)}{\partial u_k}$ is continuous.

**Assumption 3.** The DTS (3.1) satisfies a generalized Lipschitz condition, which is expressed as

$$|\Delta y_{k+1}| \leq b|\Delta u_k|$$

for any $k$ where $|\Delta u_k| \neq 0$, with $b > 0$. Here, $\Delta y_{k+1} = y_{k+1} - y_k$ and $\Delta u_k = u_k - u_{k-1}$.

**Remark 1.** From a practical standpoint, Assumption 1 serves as a fundamental prerequisite for ensuring the system's controllability. Assumption 2 implies that a finite variation in the control input does not result in an infinite variation in the system output. From an energy perspective, Assumption 3 states that the rate of change of a controller's energy cannot approach infinity if its input energy changes are finite.

**Lemma 1 [51].** Consider the nonlinear system (3.2). If $f(\cdot)$ satisfies Assumptions 1 and 2, then for $|\Delta u_k| \neq 0$, there exists a PPD $\xi_k$ and CFDL data model can be expressed as:

$$\Delta z_{k+1} = \xi_k \Delta u_k \tag{3.4}$$

where

$$\xi_k = \begin{bmatrix} \phi_{11k} & \phi_{12k} & \cdots & \phi_{1nk} \\ \phi_{21k} & \phi_{22k} & \cdots & \phi_{2nk} \\ \vdots & \vdots & \ddots & \vdots \\ \phi_{n1k} & \phi_{n2k} & \cdots & \phi_{nnk} \end{bmatrix},$$

where $||\xi_k|| \leq b$ is constrained $\forall k > 0$.

Rewriting (3.4) as:

$$z_{k+1} = z_k + \xi_k \Delta u_k \tag{3.5}$$

From (3.3), we obtain;

$$\Delta y_{k+1} = \Delta z_{k+1} + \Delta \delta_k \tag{3.6}$$

where $\Delta z_{k+1} = z_{k+1} - z_k$, and $\Delta\delta_k = \delta_k - \delta_{k-1}$. Using (3.4), (3.6) can be further written as:

$$y_{k+1} = y_k + \xi_k \Delta u_k + \Delta\delta_k \tag{3.7}$$

Let $\overline{\xi}_k =$

$$\begin{bmatrix} \phi_{11k} & 0 & 0 & \cdots & 0 \\ 0 & \phi_{22k} & 0 & \cdots & 0 \\ \vdots & \vdots & \ddots & \vdots & \vdots \\ 0 & 0 & 0 & \cdots & \phi_{nnk} \end{bmatrix}$$

Hence, (3.7) can be expressed as:

$$y_{k+1} = y_k + \overline{\xi}_k \Delta u_k + \Delta\overline{\delta}_k \tag{3.8}$$

where $\Delta\overline{\delta}_k = \sum_{j=1}^{n} \phi_{ijk} \Delta u_{jk} + \Delta\delta_k,\ i \neq j$ and $i = 1, \ldots, n$

**Remark 2.** The disturbance term $\Delta\overline{\delta}_k$, representing the coupling between control loops, disturbances, and unmodeled system dynamics, is treated as a generalized disturbance, estimated online via perturbation estimation techniques. In contrast, the dynamic linearization (DL) technique is applied to construct a virtual DL model at each sampling point, where the PPD implicitly estimates model uncertainties using I/O data.

**Remark 3.** It is important to note that the value of $\xi_k$ in (3.4) may not always align with its variation range. In other words, $\xi_k$ may satisfy, $\max \left| \frac{\xi_k - \xi_{k-1}}{t_s} \right| \leq \kappa$ where $\kappa > 0$ and $t_s$ represents the sampling interval. Consequently, $\xi_k$ can be expressed as a variable component $\vartheta_k$ combined with a constant component $\varphi$. It is important to note that $\xi_k$ may take on very small values at certain sampling times, and the parameter $\varphi$ is selected to maintain $\xi_k$ within a suitable range.

**Remark 4.** The system represented by (3.8) can be approximated to quasi-linear dynamics in local operating regions. Specifically, systems where the non-linearity can be effectively captured by the PPD representation and the Lipschitz condition holds robustly.

### 3.2.1 Perturbation Estimation

The approach employs perturbation estimation methodology [1] also in [52] as one-step delayed estimation strategy for disturbance estimation, assuming slow varying disturbance. The perturbation component $\Delta\overline{\delta}_k$ of the DTS (3.8) is evaluated as

$$
\begin{aligned}
y_{k+1} = y_k + \overline{\xi}_k \Delta u_k + \Delta\overline{\delta}_k \implies y_k = y_{k-1} + \overline{\xi}_{k-1}\Delta u_{k-1} \\
+ \Delta\overline{\delta}_{k-1} \implies \Delta\hat{\delta}_k = \Delta\overline{\delta}_{k-1} = y_k - y_{k-1} - \overline{\xi}_{k-1}\Delta u_{k-1},
\end{aligned} \tag{3.9}
$$

which allows us to rewrite (3.8) as

$$
y_{k+1} = y_k + \overline{\xi}_k \Delta u_k + \Delta\hat{\delta}_k - \Delta\tilde{\delta}_k, \tag{3.10}
$$

where $\Delta\tilde{\delta}_k = \Delta\hat{\delta}_k - \Delta\overline{\delta}_k$ represents the perturbation assessment error. Thus,

$$
\begin{aligned}
\Delta\tilde{\delta}_k = \Delta\overline{\delta}_{k-1} - \Delta\overline{\delta}_k = [(y_k - y_{k-1}) - (y_{k+1} - y_k) \\
- \xi_{k-1}\Delta u_{k-1} + \overline{\xi}\Delta u_k].
\end{aligned}
$$

Based on Assumption 1 and Lemma 1, it is established that $y_k$, $u_k$, and $\overline{\xi}_k$ are bounded. Consequently, it can be inferred that $\Delta\tilde{\delta}_k$ is also bounded.

**Remark 5.** It performs well when disturbances change linearly or predictably over time. Due to its simple architecture and exceptional performance, perturbation estimation has found widespread use in different control systems.

### 3.2.2 Pseudo Partial Derivative Assessment

The index function for the unknown PPD estimation, as given in [14], is used in this chapter as

$$
J(\hat{\xi}_k) = \left\| y_k - y_{k-1} - \hat{\xi}_k \Delta u_{k-1} \right\|^2 + \nu \left\| \hat{\xi}_k - \hat{\xi}_{k-1} \right\|^2 \tag{3.11}
$$

where $\hat{\xi}_k$ is the estimated value of $\overline{\xi}_k$. Setting $\frac{\partial J}{\partial \hat{\xi}_k} = 0$, we obtain

$$
\begin{aligned}
\hat{\xi}_k &= \hat{\xi}_{k-1} + \frac{\Pi \Delta u_{k-1}^T}{\nu + \Delta u_{k-1}^2} \left[ \Delta y_k - \hat{\xi}_{k-1} \Delta u_{k-1} \right], \\
\hat{\phi_{ii}}_k &= \hat{\phi}_{ii}(1), \text{ if } |\hat{\phi_{ii}}_k| \leq \epsilon.
\end{aligned} \tag{3.12}
$$

$\nu > 0$, $\Pi \in (0, 1]$, and $\epsilon > 0$ is sufficiently small. Here $\hat{\phi}_{ii}(1) > 0$ is the initial value of $\hat{\phi_{ii}}_k$. Let us define $\hat{\xi}_k = \hat{\vartheta}_k + \varphi$. Then, (3.10) can be further written as

$$
y_{k+1} = y_k + (\hat{\vartheta}_k + \varphi_)\Delta u_k + \Delta\hat{\delta}_k - \Delta\tilde{\delta}_k \tag{3.13}
$$

where $\hat{\vartheta}_k$ can be obtained using (3.12), and $\varphi = \text{diag}\{\varphi_1, \varphi_2, \ldots, \varphi_n\}$. The elements of $\varphi$ are taken as a non-negative constant.

**Remark 6.** To guarantee the feasibility of the adaptive law (3.13), $\nu$ should be selected to be smaller than the magnitude of $\Delta u_k$.

**Remark 7.** The updating law (3.13) is designed based solely on the controlled system's input and output measurement data, without reliance on the model's structural and dynamic information.

**Remark 8.** At certain sampling instances, the diagonal element $\hat{\bar{\xi}}_k$ may become exceedingly small. Consequently, the parameter $\varphi$ is chosen to ensure that $\hat{\bar{\xi}}_k$ remains within an acceptable range.

## 3.3 Minimum Operator Based CFDL-DSMC Design

This section outlines the controller design process of the MDSMC-CFDL scheme. A data-driven controller is derived from the CFDL data model and the MDSMC scheme, and the stability of the proposed control method is also demonstrated. Further development is presented for the SISO case; however, the MIMO case will follow the same approach.

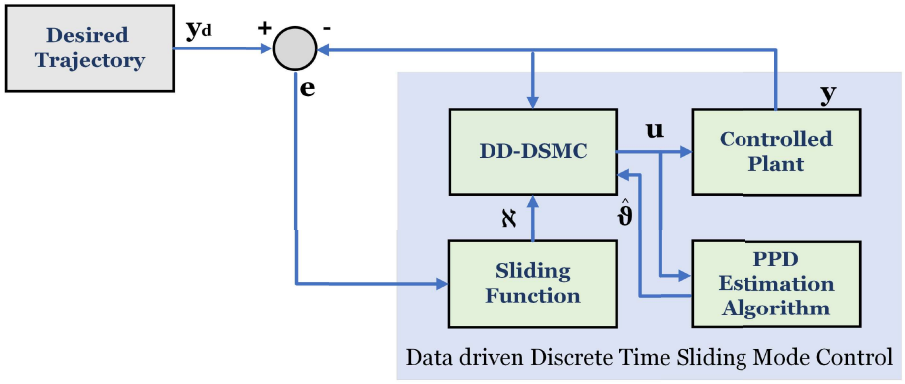


Figure 3.1: Flow chart of MDSMC-CFDL scheme.

### 3.3.1 Design of Controller Using CFDL-RL1 Scheme

Define the tracking error as follows:

$$e_k = y_k - y'_k \tag{3.14}$$

where $y_k$ represents the system output signal and $y'_k$ denotes the bounded desired input signal. Define the sliding function as

$$\aleph_k = \lambda_1 e_k \tag{3.15}$$

The CFDL-RL1-based control strategy can be obtained using [2] as shown below:

$$\aleph_{k+1} = \lambda_1 e_{k+1} = \lambda_1[y_{k+1} - y'_{k+1}]$$
$$\aleph_k - \text{sign}[\aleph_k] \min(|\aleph_k|, \varsigma) = \lambda_1[y_k + (\hat{\vartheta}_k + \varphi)\Delta u_k + \Delta\hat{\delta}_k - \Delta\tilde{\delta}_k - y'_{k+1}]$$

The control can be obtained as

$$\Delta u_k = \frac{\eta^T}{\eta\eta^T}(\aleph_k - \text{sign}[\aleph_k] \min(|\aleph_k|, \varsigma) - \lambda_1(y_k - \Delta\hat{\delta}_k + \Delta\delta_k + y'_{k+1})$$

Here, $\eta = \lambda_1(\hat{\vartheta}_k + \varphi)$, further to implement the controller, the future reference position $y'_{k+1}$ is required. In practice, the desired trajectory is typically predefined within the control system, making $y'_{k+1}$ available.

$$\Delta u_k = \frac{\eta^T}{\eta\eta^T}(\aleph_k - \text{sign}[\aleph_k] \min(|\aleph_k|, \varsigma) - \lambda_1(y_k - \Delta\hat{\delta}_k + y'_{k+1}) \tag{3.16}$$

It is important to note that the control law in equation (3.16) is derived under the assumption that $\Delta\tilde{\delta}_k$ is accurately estimated, specifically $\Delta\tilde{\delta}_k = 0$. However, $\Delta\tilde{\delta}_k \neq 0$. To ensure robustness against errors in disturbance estimation, the parameter $\varsigma$ should satisfy the following condition:

$$\varsigma > \omega_m \geq \|\Delta\hat{\delta}_k\| \tag{3.17}$$

### 3.3.2 Design of Controller Using CFDL-RL2 Scheme

Consider the same tracking error and the sliding function as defined in (3.14) and (3.15), respectively. The CFDL-RL2-based control strategy can be obtained using [2] as shown below:

$$\aleph_{k+1} = \lambda_1 e_{k+1}$$
$$\aleph_k - \varsigma\text{sign}[\aleph_k] \min\left(\frac{|\aleph_k|}{\varsigma}, |\aleph_k|^\beta\right) = \lambda_1[y_{k+1} - y'_{k+1}]$$
$$\aleph_k - \varsigma\text{sign}[\aleph_k] \min\left(\frac{|\aleph_k|}{\varsigma}, |\aleph_k|^\beta\right) = \lambda_1[y_k + (\hat{\vartheta}_k + \varphi)\Delta u_k + \Delta\hat{\delta}_k - \Delta\tilde{\delta}_k - y'_{k+1}]$$

The control can be obtained as

$$\Delta u_k = \frac{\eta^T}{\eta\eta^T}(\aleph_k - \varsigma \text{sign}[\aleph_k] \min\left(\frac{|\aleph_k|}{\varsigma}, |\aleph_k|^\beta\right) - \lambda_1(y_k - \Delta\hat{\delta}_k + y'_{k+1}) \tag{3.18}$$

**Remark 11.** In control law (3.18), setting $\varsigma$ to 1 and keeping $\beta$ very close to zero results in behavior similar to control law (3.16) with $\varsigma = 1$. The interaction between $\varsigma$ and $\beta$ influences the convergence of the switching function. Smaller values of $\varsigma$ and $\beta$ lead to slower convergence, while keeping $\beta$ close to 1 and $\varsigma$ large ensures rapid convergence of the switching function. Furthermore, the selection of $\varsigma$ and $\beta$ for various applications can be tailored based on the actuator saturation limits of the respective systems.

### 3.3.3 Stability Analysis

**Lemma 2.** If the nonlinear system described in equation (3.1) satisfies Assumptions 1 to 3 and is controlled using the CFDL-RL1 algorithm using (3.16), with the desired signal $y'_{k+1}$ being bounded, then the estimated value $\hat{\xi}_k$ will also be bounded.

**Proof** Considering the PPD estimation algorithm, we have two scenarios;

*Case 1*: if $\hat{\phi}_{iik} \leq \epsilon$, this will ensure $\hat{\phi}_{iik} = \hat{\phi}_{ii}(1)$, and $\hat{\xi}_k$ will be bounded.

*Case 2*: if $\hat{\phi}_{iik} > \epsilon$, using (3.12) we have:

$$\tilde{\xi}_k = \Delta\xi_k + \left(1 - \frac{\Pi\Delta u_{k-1}^2}{\nu + \Delta u_{k-1}^2}\right)\tilde{\xi}_{k-1}$$

Using Lemma 1, we have $||\xi_k|| \leq b$, and

$$\left\|\tilde{\xi}_k\right\| < \left\|\left(1 - \frac{\Pi\Delta u_{k-1}^2}{\nu + \Delta u_{k-1}^2}\right)\right\| \left\|\tilde{\xi}_{k-1}\right\| + 2b$$

Considering (3.19), we have

$$\Pi\Delta u_{k-1}^2 < \Delta u_{k-1}^2 < \nu + \Delta u_{k-1}^2$$

Here, $\nu > 0$ and $\Pi \in (0, 1]$, Therefore, there exists a positive constant $\gamma \in (0, 1]$, leading to the following:

$$0 < 1 - \frac{\Pi\Delta u_{k-1}^2}{\nu + \Delta u_{k-1}^2} \leq \gamma < 1$$

Thus, we have:

$$\left\|\tilde{\xi}_k\right\| \leq \gamma \left\|\tilde{\xi}_{k-1}\right\| + 2b \leq \gamma^2 \left\|\tilde{\xi}_{k-2}\right\| + 2 + 2b$$

$$\leq \cdots \leq \gamma^k \left\| \tilde{\xi}(0) \right\| + 2b\frac{(1-\gamma^k)}{1-\gamma}$$

it follows that $\tilde{\xi}_k$ is bounded. Consequently, $\hat{\xi}_k$ is also bounded.

**Theorem 1.** If Assumptions 1 to 3 are satisfied for the system (3.1) the controller described by (3.16) and (3.17) is used and the time-dependent term $\Delta\hat{\delta}_k$ and $\hat{\xi}_k$ are updated according to equations (3.10) and (3.12), then the QSM will converge in a finite number of steps.

**Proof** From (3.15) we have,

$$\aleph_{k+1} = \lambda_1 e_{k+1}$$

using (3.14) and (3.15), we have

$$\begin{aligned}\aleph_{k+1} = \lambda_1 e_{k+1} &= \lambda_1[y_{k+1} - y'_{k+1}] \\ &= \lambda_1[y_k + (\hat{\vartheta}_k + \varphi)\Delta u_k + \Delta\hat{\delta}_k - \Delta\tilde{\delta}_k \\ &- y'_{k+1}]\end{aligned}$$

When applying control law (3.16), the system follows

$$\aleph_{k+1} = -\Delta\tilde{\delta}_k + \aleph_k - \text{sign}[\aleph_k]\min(|\aleph_k|, \varsigma)$$

From, (3.17) we have

$$-\omega_m < \Delta\tilde{\delta}_k < \omega_m \tag{3.19}$$

Hence, when $\aleph_0 \leq \varsigma$ using (3.17) we have the next step as $-\varsigma < \aleph_{k+1} < \varsigma$, Hence meeting definition 2 and for $k = \mathcal{T}(\aleph_0) = 1$, we have $\aleph_{k+1} \leq \omega_m$. Here $\omega_m$ is defined as (3.17) and $\mathcal{T}(\aleph_0)$ is a settling time function. Now, if we have the scenario, $\aleph_0 > \varsigma$

$$\aleph_{k+1} = -\Delta\tilde{\delta}_k + \aleph_k - \varsigma$$

$$-2\varsigma < \aleph_{k+1} - \aleph_k < 0 \tag{3.20}$$

Hence, meeting definition 2. Also,

$$\begin{aligned}\aleph_{k+1} &\leq \aleph_k - \varsigma + \omega_m \\ \aleph_k &\leq \aleph_{k-1} - (\varsigma - \omega_m) \\ &\vdots \\ &\leq \aleph_0 - k(\varsigma - \omega_m)\end{aligned}$$

and for some $k = \mathcal{T}(\aleph_0) = \lceil \frac{\aleph_0 - \omega_m}{\varsigma - \omega_m} \rceil$, we have $\aleph_{k+1} \leq \omega_m$. Here, $\omega_m$ is defined as (3.17). Thus, it can be inferred that the modulus of the switching function reaches an ultimate bound of $\omega_m$, attained within a finite number of steps.

**Lemma 3.** If the nonlinear system described in equation (3.1) satisfies Assumptions 1 to 3 and is controlled using the CFDL-RL2 algorithm using (3.18), with the desired signal $y'_{k+1}$ being bounded, then the estimated value $\hat{\xi}_k$ will also be bounded.

**Proof** Using (3.18), the proof will follow a similar approach to that of Lemma 2.

**Theorem 2.** If Assumptions 1 to 3 are satisfied for the system (3.1) the controller described by (3.18) and (3.19) is used and the time-dependent term $\Delta\hat{\delta}_k$ and $\hat{\xi}_k$ are updated according to equations (3.10) and (3.12), then the QSM will converge in a finite number of steps.

**Proof** From (3.15) we have,

$$\aleph_{k+1} = \lambda_1 e_{k+1}.$$

Using (3.14) and (3.15), we have

$$\begin{aligned}\aleph_{k+1} = \lambda_1 e_{k+1} &= \lambda_1[y_{k+1} - y'_{k+1}] \\ &= \lambda_1[y_k + (\hat{\vartheta}_k + \varphi)\Delta u_k + \Delta\hat{\delta}_k - \Delta\tilde{\delta}_k - y'_{k+1}]\end{aligned}$$

When applying control law (3.18), the system follows

$$\aleph_{k+1} = -\Delta\tilde{\delta}_k + \aleph_k - \varsigma \text{sign}[\aleph_k] \min\left(\frac{|\aleph_k|}{\varsigma}, |\aleph_k|^\beta\right)$$

when $\frac{\aleph_0}{\varsigma} \leq |\aleph_0|^\beta$ using (3.17) we have the next step as $-\varsigma < \aleph_{k+1} < \varsigma$

Hence, meeting definition 3 and for $k = \mathcal{T}(\aleph_0) = 1$, we have $\aleph_{k+1} \leq \omega_m$. Here $\omega_m$ is defined as (3.17) and $\mathcal{T}(\aleph_0)$ is a settling time function. Now, if we have the scenario $\frac{\aleph_0}{\varsigma} > |\aleph_0|^\beta$

$$\begin{aligned}\aleph_{k+1} &= -\Delta\tilde{\delta}_k + \aleph_k - \varsigma\, \text{sign}(\aleph_k)|\aleph_k|^\beta \\ \Rightarrow |\aleph_{k+1}| &\leq |\aleph_k| - \varsigma|\aleph_k||\aleph_k|^\beta + \omega_m\end{aligned}$$

proceeding ahead with $|\aleph_k|$, we have

$$\begin{aligned}|\aleph_k| &\leq |\aleph_{k-1}|(1-\varsigma|\aleph_{k-1}||\aleph_{k-1}|^{\beta-1}+\omega_m|\aleph_{k-1}|^{-1}) \\ &\vdots \\ &\leq |\aleph_0|(1 - \varsigma|\aleph_0||\aleph_0|^{\beta-1} + \omega_m|\aleph_0|^{-1}) \ldots \\ &(1 - \varsigma|\aleph_{k-1}||\aleph_{k-1}|^{\beta-1} + \omega_m|\aleph_{k-1}|^{-1})\end{aligned}$$

$$|\aleph_k| \leq |\aleph_0|(1-\varsigma|\aleph_0||\aleph_0|^{\beta-1}+\omega_m|\aleph_0|^{-1})^k \tag{3.21}$$

Now, at a certain $k$, we will have the scenario

$$|\aleph_0|\left(1-\varsigma|\aleph_0|^{\beta-1}+\omega_m|\aleph_0|^{-1}\right)^k \leq \varsigma|\aleph_k|^{\beta}.$$

Using (3.21), we have, $|\aleph_k| \leq \varsigma|\aleph_k|^{\beta} \implies |\aleph_{k+1}| \leq \omega_m$.

Therefore,

$$|\aleph_{k+1}| \leq \omega_m, \quad \forall k \geq \left\lceil \log_{[1-\varsigma|\aleph_0|^{-1}+\omega_m|\aleph_0|^{-1}]} \frac{\varsigma^{\frac{1}{1-\beta}}}{|\aleph_0|} \right\rceil,$$

and for some $k = \mathcal{T}(\aleph_0)$, we have

$$\mathcal{T}(\aleph_0) = \left\lceil \log_{[1-\varsigma|\aleph_0|^{-1}+\omega_m|\aleph_0|^{-1}]} \frac{\varsigma^{\frac{1}{1-\beta}}}{|\aleph_0|} \right\rceil.$$

Thus, it can be inferred that the modulus of the switching function reaches an ultimate bound of $\omega_m$, attained within a finite number of steps.

## 3.4 Result and Discussion

To validate the performance of the CFDL-RL1 and CFDL-RL2 control schemes, this section presents numerical simulation using a nonlinear system example and experimental validation of the same on a coupled tank system test bench. Additionally, to highlight the characteristics of the proposed method, numerical comparisons are made with CFDL-DITSMC [1] for both proposed algorithms.

### 3.4.1 Numerical Simulation

Consider the SISO DTS given by

$$y_{k+1} = \frac{y_k\ y_{k-1}\ y_{k-2}\ u_{k-1}\,(y_{k-2}-1)+u_k}{1+y_{k-1}^2+y_{k-2}^2} + d_k$$

where $d_k$ represents the external perturbation, defined as

$$d_k = \left[0.5, 0.15\sin\left(\frac{k}{30}\right)\right][y_k, y_{k-1}]^T \tag{3.22}$$

The initial states are defined as $u(1:2) = 0$, $y(1:3) = 0$, $\hat{\vartheta}(1:2) = 2$, and $\epsilon = 10^{-5}$. The resetting value $\hat{\vartheta}(1)$ is set to 0.5, and the CFDL-DITSMC [1] terms are chosen as

$\nu = 0.5$, $\Pi = 0.3$, $\lambda_s = 0.0002$, $\lambda_1 = 0.3$, $\lambda_2 = 0.2$, $\alpha = \frac{5}{7}$, $\omega = 0.01$, $\Delta = 0.002$, $\delta = 3$, and $\epsilon = 10^{-5}$. The reference signal $y'_k$ is given as

$$y_{rk} = \begin{cases} 0.5, \ k < 500 \\ 0.8, \ k \geq 500 \end{cases}$$

The coefficients $\lambda_1$ for RL1 and RL2 is considered as 1.1 and $\beta = 0.1$ for RL2. Fig. 3.2 presents the numerical simulation results using the RL1 scheme.Fig. 3.3b presents control input, and Fig. 3.3a represents disturbance estimation error, which is significantly lower than previous work. In Fig. 3.2a, the tracking error remains bounded and exhibits a reduced QSMD compared to the CFDL-DITSMC method. Additionally, Fig. 3.2b illustrates that the output successfully tracks the reference signal within a finite time.

Simulation results using RL2 scheme are shown in Fig. 3.3. The output successfully tracks the reference signal, and the error shows reduced QSMD, as shown in Fig. 3.4b and Fig. 3.4a, respectively. Consequently, the proposed method exhibits improved performance in both tracking accuracy and error reduction.

### 3.4.2 Experimental Validation

The coupled tank system is used as a test bench. The schematic in Fig. 3.6a illustrates the construction of the system, and Fig. 3.6 shows the actual test bench, where the control objective is to maintain the desired water level in tank 2. Configuration 2 of the coupled tank system [53] is chosen for the experiments. In this configuration, the control input is applied to the inlet of tank 1, and the outflow of tank 1 acts as a control for tank 2. This setup introduces a coupling effect, where the levels in both tanks are interdependent, adding complexity to the control process. The liquid level is measured by a pressure sensor at the bottom of each tank, providing a linear voltage output that increases with pressure. This signal is processed through a conditioning board and converted to a 0 to $5V$ DC output. The control parameters used for the experimental setup are $\beta = 0.1$, $\lambda_1 = 0.3$, $\lambda_2 = 0.3$ and $\varsigma = 1$. For the system parameters, reader may refer to [53]. The reference water level to track for MRL1 scheme is given as

$$y_r = \begin{cases} 4 \text{ cm}, \ t < 400 \text{ sec} \\ 7 \text{ cm}, \ t \geq 400 \text{ sec} \end{cases}$$

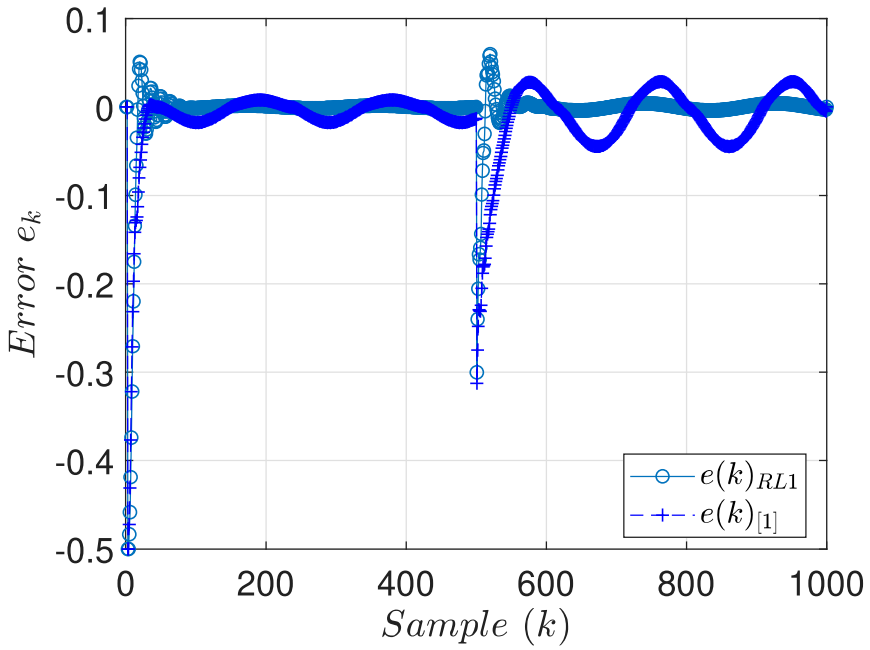


(a) CFDL-RL1 Trajectory error e(k)

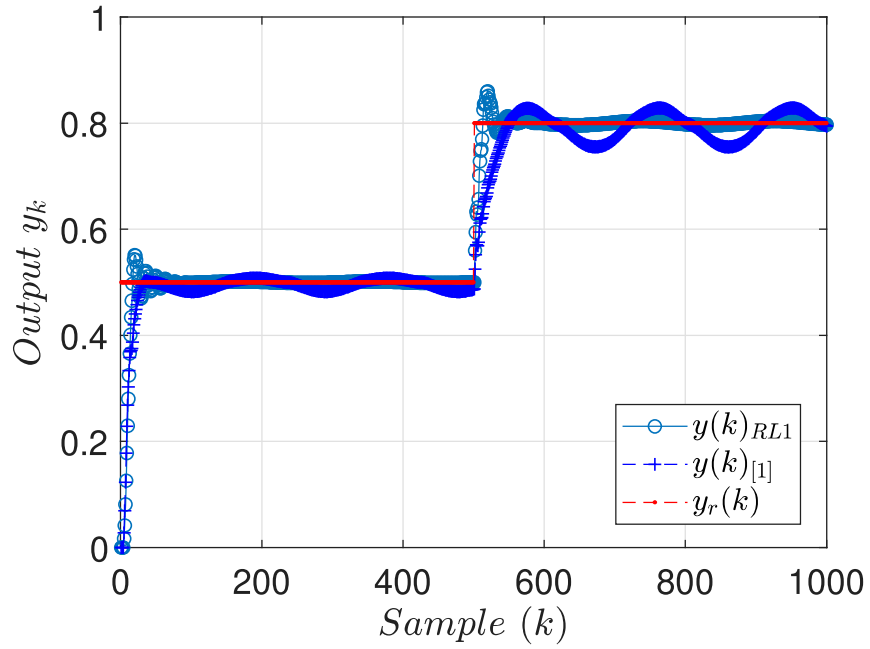


(b) CFDL-RL1 output

Figure 3.2: Comparison of trajectory error and output for CFDL-RL1 with [1] .

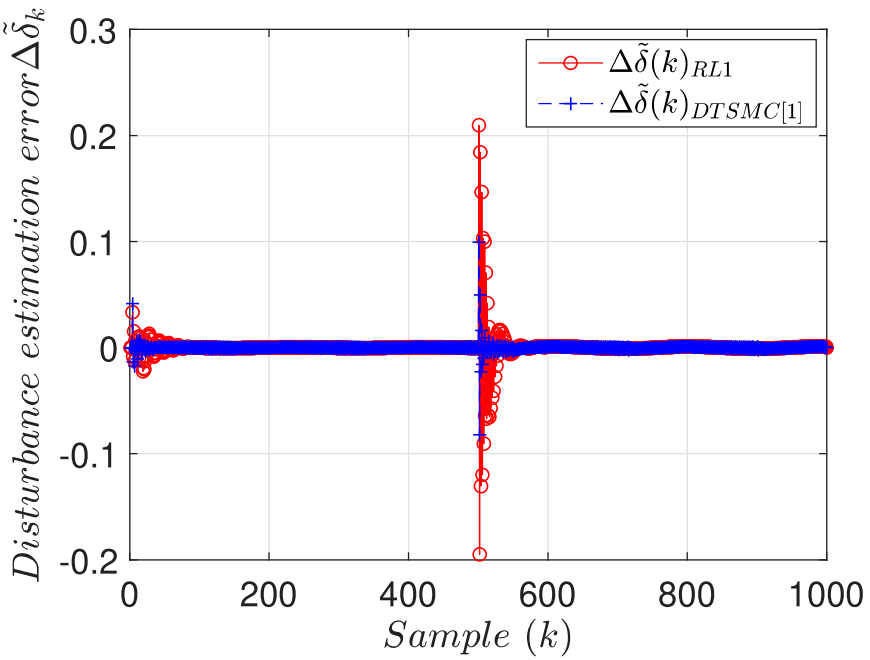


(a) CFDL-RL1 disturbance error estimation $\Delta\hat{\delta}_k$

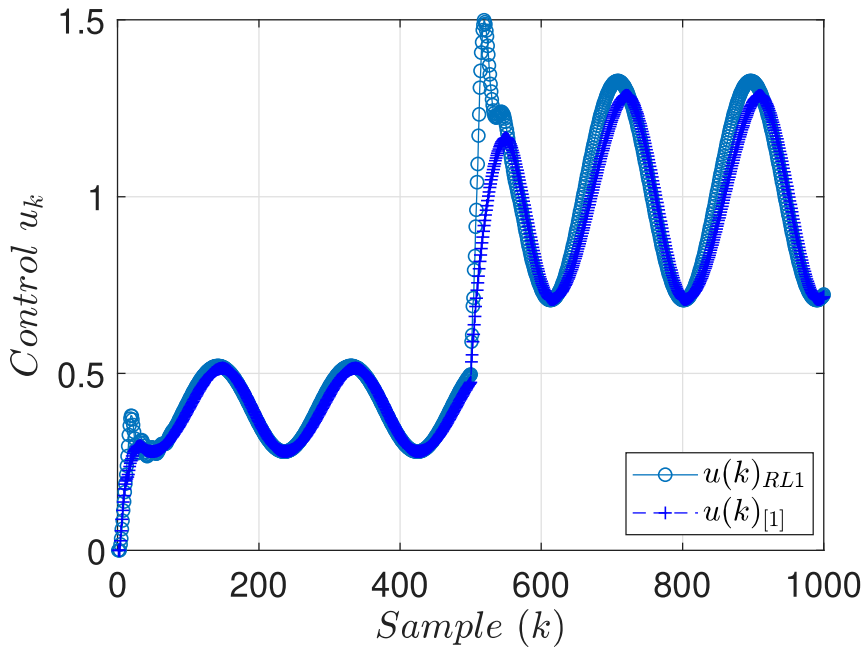


(b) CFDL-RL1 Control input u(k)

Figure 3.3: Comparison of control performance and disturbance estimation for CFDL-RL1 with [1].

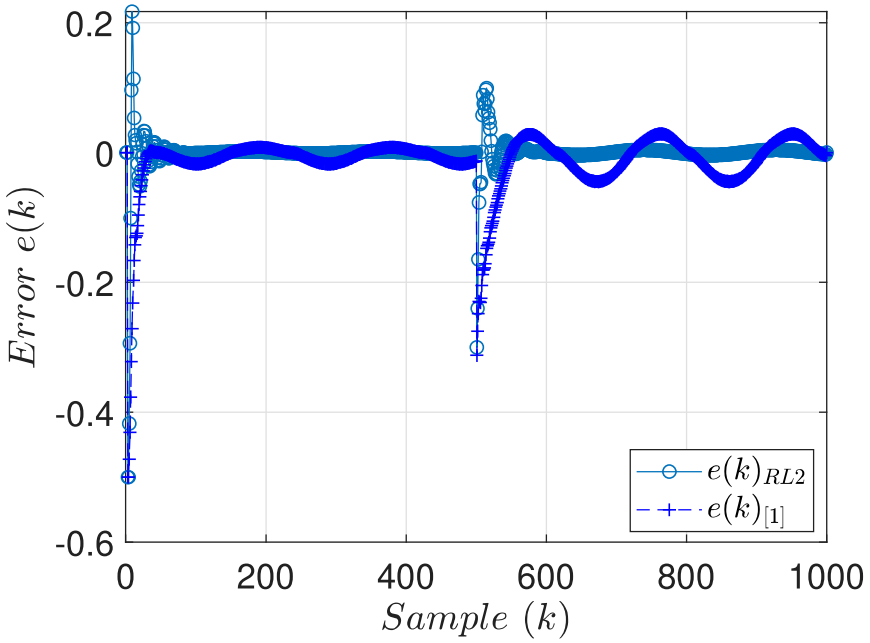


(a) CFDL-RL2 Trajectory error e(k)

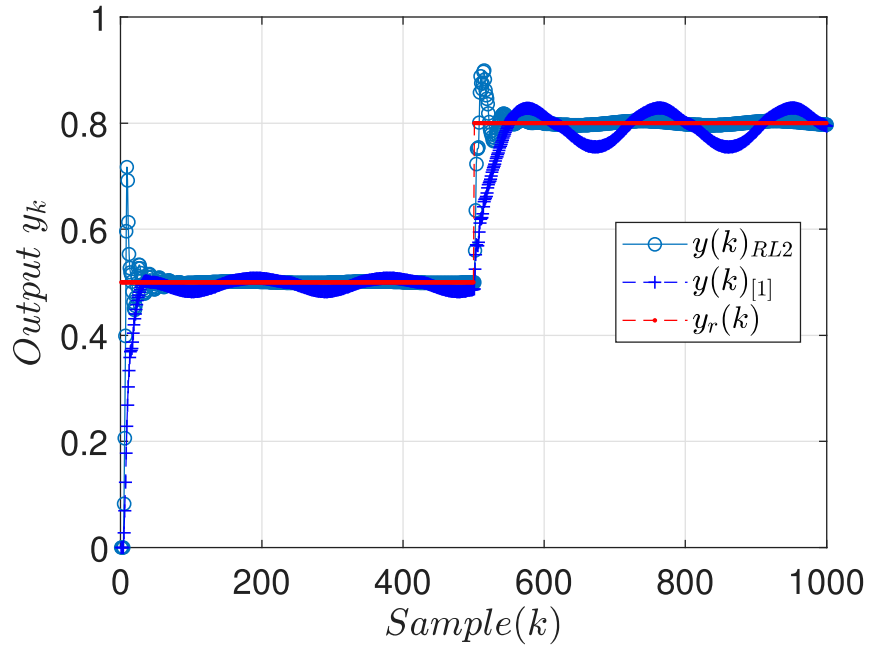


(b) CFDL-RL1 output

Figure 3.4: Comparison of trajectory error and output for CFDL-RL2 with [1].

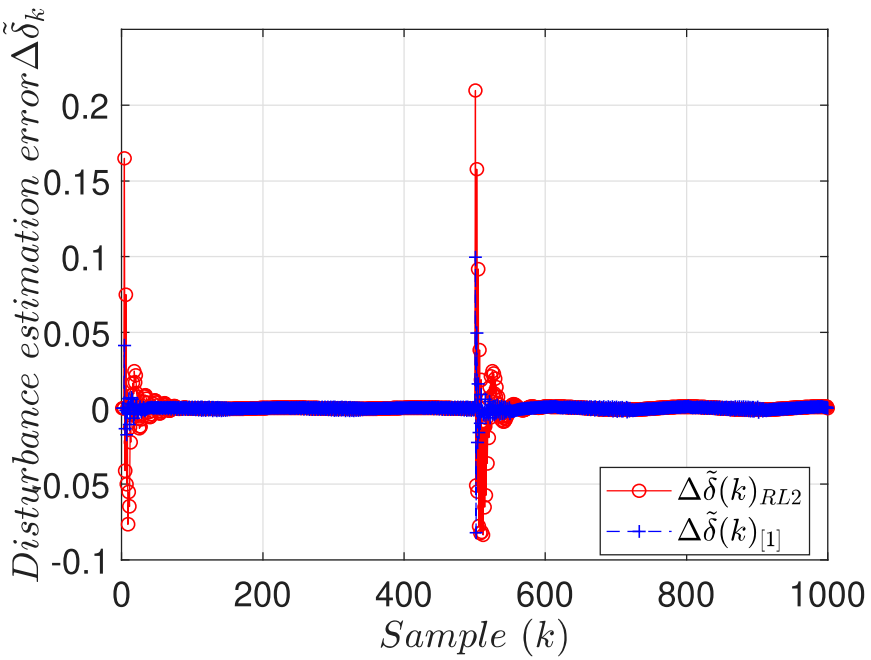


(a) CFDL-RL2 disturbance error estimation $\Delta\hat{\delta}_k$

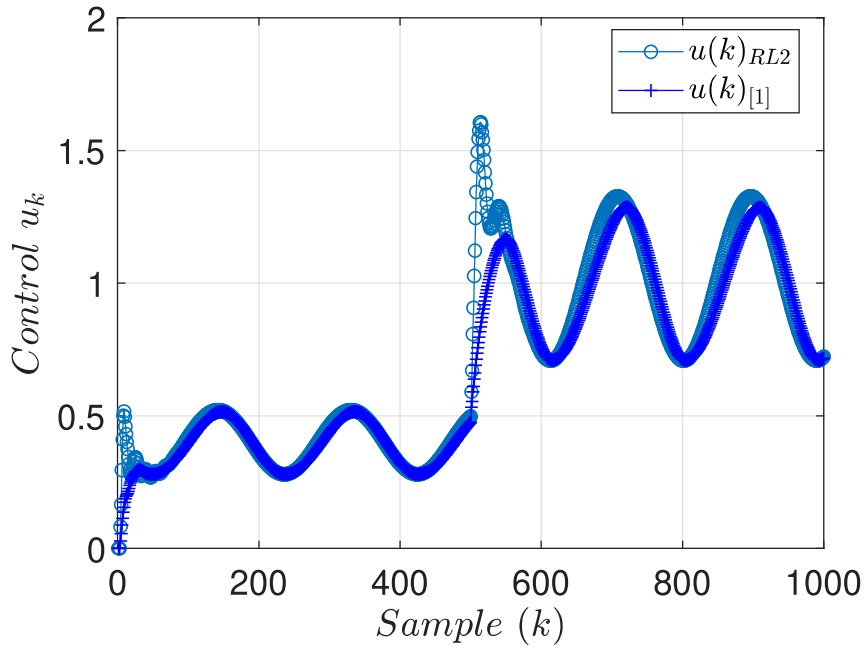


(b) CFDL-RL2 Control input u(k)

Figure 3.5: Comparison of control performance and disturbance estimation for CFDL-RL2 with [1].

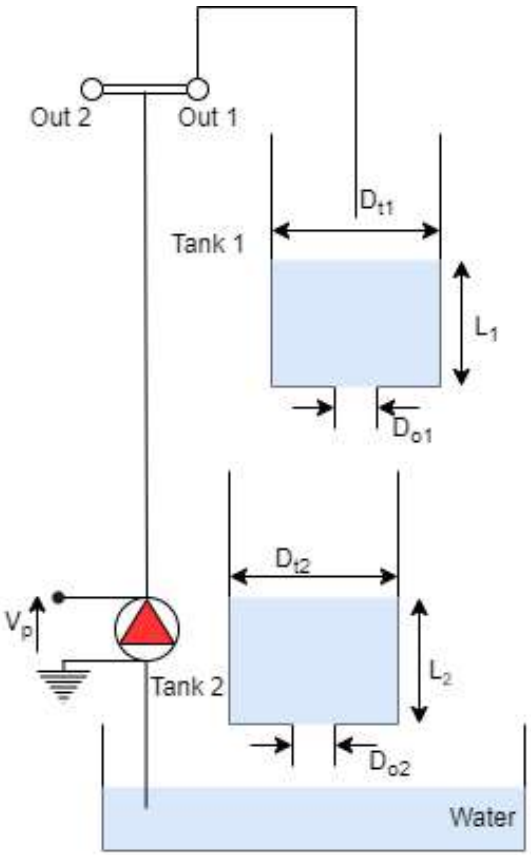


(a) Coupled tank block diagram

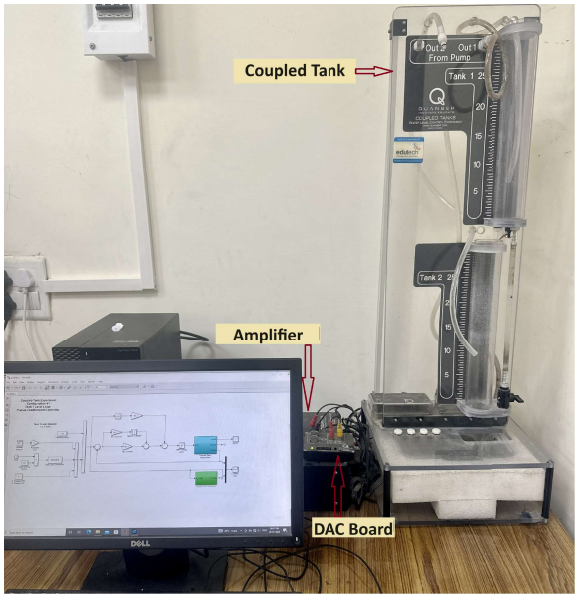


(b) Coupled tank setup

Figure 3.6: Coupled tank system

Fig. 3.7a shows the experimental validation of the proposed MRL1 scheme where the reference levels are achieved in finite time. Fig. 3.7b shows the control input. Similarly, for MRL2 scheme, the reference level is set as

$$y_r = \begin{cases} 7 \text{ cm}, \ t < 400 \text{ sec} \\ 8 \text{ cm}, \ t \geq 400 \text{ sec} \end{cases}$$

Fig. 3.8a depicts the experimental validation of the proposed MRL2 scheme, and Fig. 3.8b shows the control input.

## 3.5 Conclusion

This chapter introduces two innovative DDC control schemes designed for discrete-time systems subjected to disturbances. By utilizing the CFDL technique and incorporating MDSMC methods, these schemes effectively mitigate QSMB and achieve finite-time tracking for model-free systems. Compared to existing methods, the proposed approaches are simpler and more robust due to their reliance on fewer tuning parameters. The effectiveness of the CFDL–MDSMC framework is demonstrated through numerical simulations and experimental validation on a liquid-level control system. Numerical results show improved disturbance rejection and finite-time convergence, while experimental findings confirm the practical feasibility and robustness of the proposed control schemes in real-world applications. The proposed DDC control schemes achieve finite-time convergence under disturbances while minimizing the required design parameters, making them highly suitable for complex, nonlinear systems, particularly in scenarios where system models are unavailable. Their successful implementation on a liquid-level control system highlights their potential for broader adoption across industrial and engineering applications.

As part of future work, we plan to extend this study to highly uncertain or weakly observable systems, thereby broadening the scope and applicability of the proposed framework. In addition, broader generalizability across different scenarios should be established with a focus on persistence of excitation, actuator wear, and the energy of the control signal.

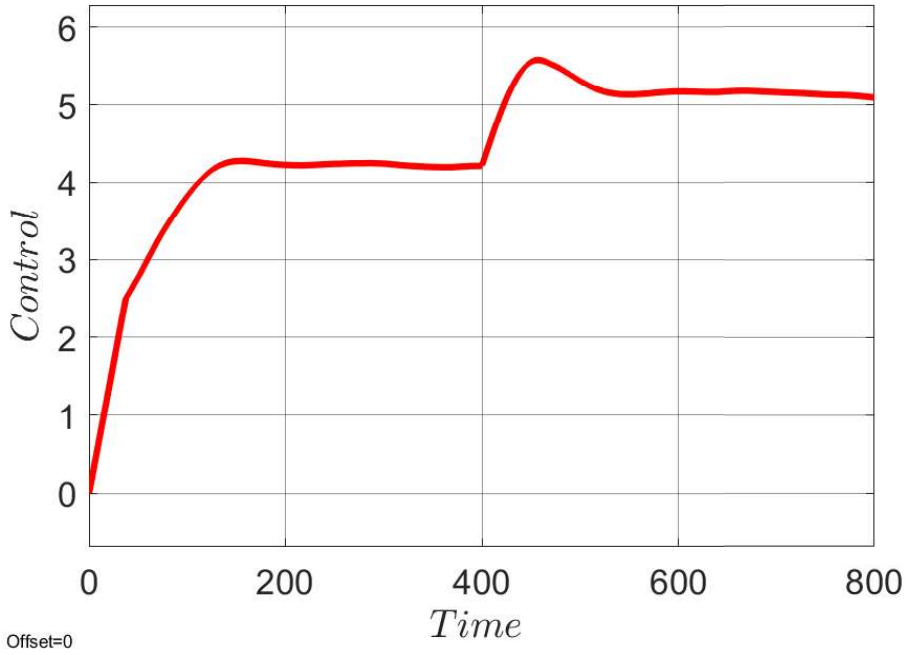


(a) Results of CFDL-RL1 scheme output,

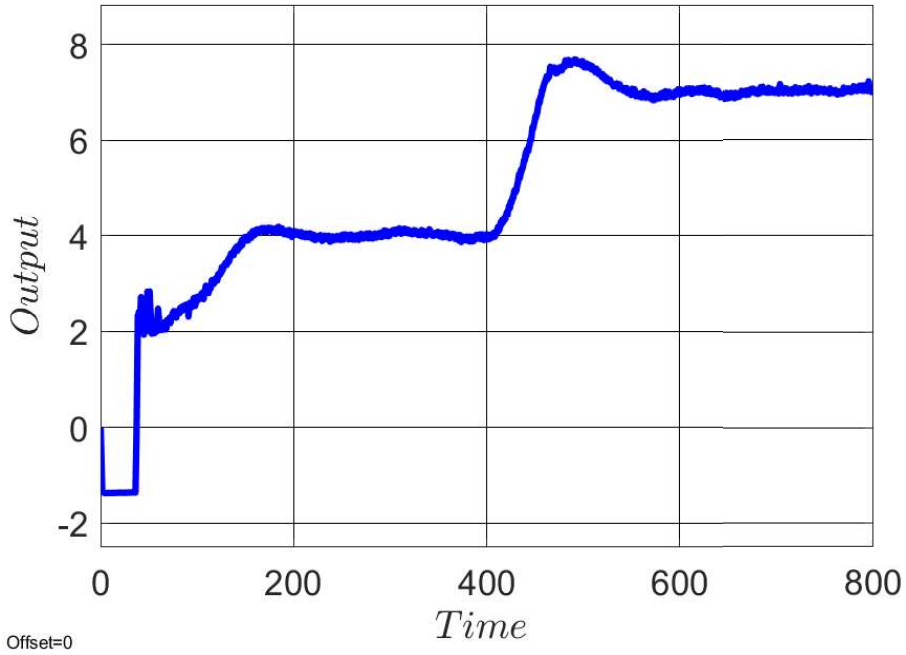


(b) Results of CFDL-RL1 scheme control input,

Figure 3.7: Overview of the experimental results for CFDL-RL1

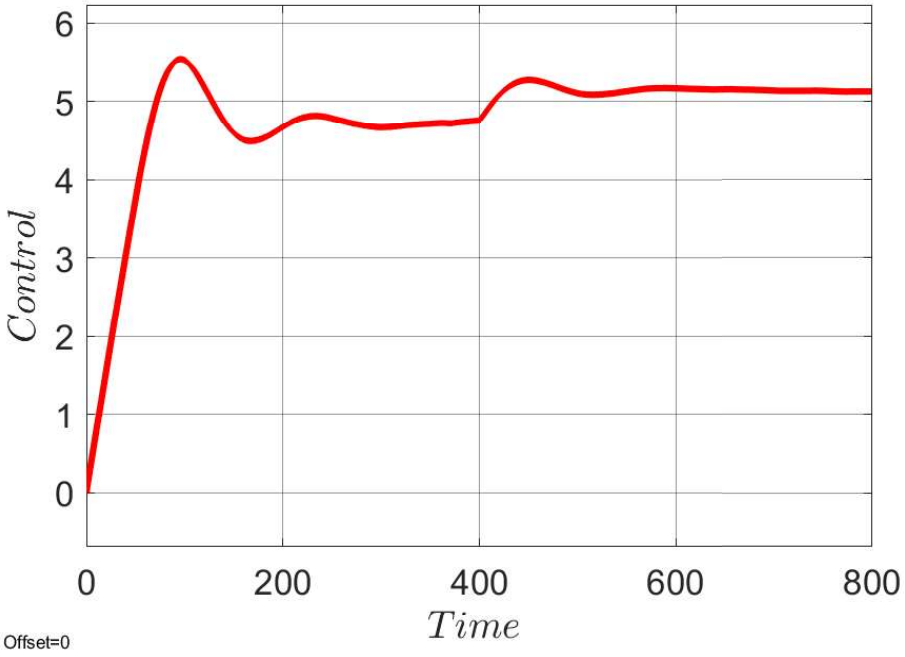


(a) Results of CFDL-RL2 scheme output

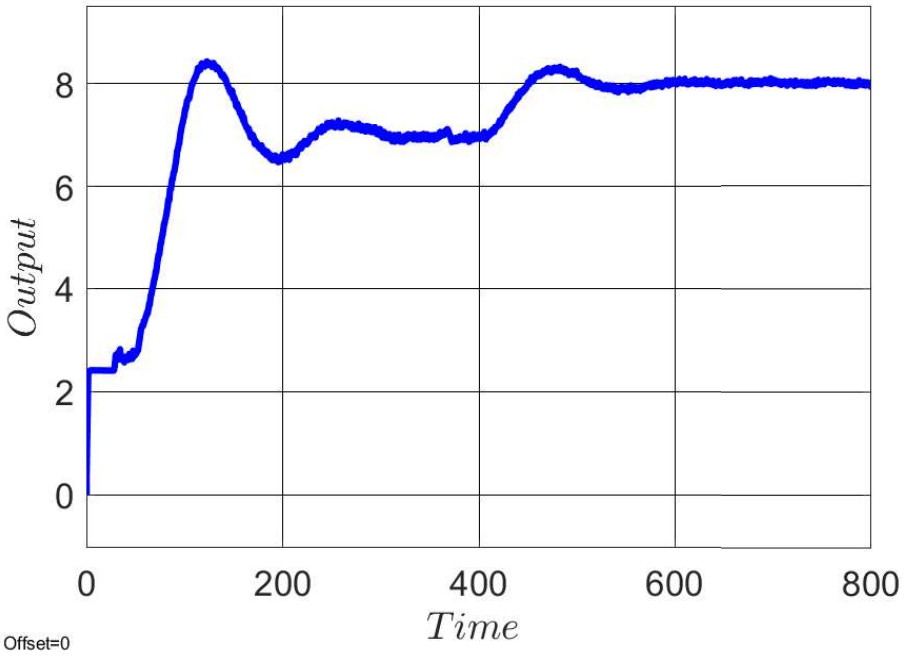


(b) Results of CFDL-RL2 scheme control input.

Figure 3.8: Overview of the experimental results for CFDL-RL2